Finite Radon Transform as Subcarriers Mapping Technique for OFDM System

Khalid G Samarah

Abstract—**Radon Transform (RT) becomes a mathematical basis for solving computerized tomography, and finds application in medical imaging and image processing. Finite groups represent digital images; the Finite Radon Transform (FRAT) is then applied. To overcome the periodization effect of a finite transform, Do and Vetterli [1] introduce a novel ordering of the FRAT coefficients. This paper introduced a detailed mathematical analysis of the optimal ordering of FRAT coefficients that introduces new normal vectors that are clearly identified with examples producing the FRAT transform. Lately FRAT is used with OFDM systems as an M-Ary mapping technique, thus, the signal constellation of some of the different orders of FRAT is presented as well as generating the OFDM symbols from the output of FRAT. This procedure leads to extra investigation on the performance of FRAT-based OFDM systems in comparison with the QAM mapping techniques.**

Key Words— **Finite Radon Transform, FRAT, M-Ary Mapping, Radon, OFDM.**

I. INTRODUCTION

In 1917, Johann Radon presented a solution to the inversion of linear function transformation and a solution of the dual problem of calculating a line function from its point mean values [2]. His solution is later known as the Radon Transform (RT), which becomes a mathematical basis for solving computerized tomography, and finds application in medical imaging and image processing [3, 4].

There is a powerful relationship between the Radon transform (RT) and the Fourier transform. Deans book is considered as a perfect literature for the researchers who are interested in obtaining wide information about this topic [5]. This important result, known as the central-slice or projection-slice theorem, shows that the 1D Fourier transform of a projection of a 2D function is directly one line through the 2D Fourier transform of the function itself [3, 5-8]. The Fourier transform (FT) characterizes the overall regularity of a periodic signal as well as the related concept of frequency scale. The orthogonality of the basic functions, which allows for a unique signal decomposition, is an important feature of FT. thus, it is used as the major part of generating the OFDM symbols used

as the air interface for the next generation of mobile systems [9-11]. The essential relationship between the Fourier transform and the Radon transform is given as follows:

$$\mathcal{R} = \mathcal{R}\{f\} = \mathcal{F}_{1D}^{-1}\{\mathcal{F}_{2D}\{f\}\} \qquad (1)$$

Fig. 1 displays the corresponding graphical interpretation [5, 12]. A new algorithm based on the generalized Radon transform that works on binary images, obtained by deconvolution is proposed in [13] for fast curve parameter estimation.

The fundamental idea is to reduce the computational cost of the generalized Radon transform by the use of a precondition map. To generate the precondition map, a fast mapping procedure named image point mapping is developed [13]. Beylkin in [7] describes the discrete RT (DRT) and the exact inversion of it. The DRT is a very useful tool for multidimensional DSP and other applications of digital signals and image processing described in [7, 14-20].
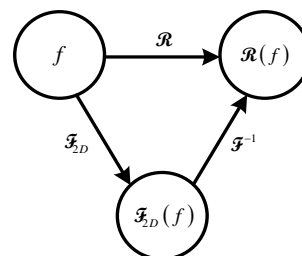

Fig. 1. The Relation between Radon Transform and Fourier Transform

Section II introduces the Radon Transform with clear description of the generating the sinogram from the different projections, which introduces Fourier Slice Theorem presented in section III. Section IV describes in details the Finite Radon Transform applied to finite groups represent digital images. A novel ordering of the FRAT coefficients is introduced by Do and Vetterli [1] with examples to simply clarify the procedure of reordering the coefficients. Assuming binary input to the FRAT transform and the inverse of the FRAT transform are introduced as well. The resulted complex symbols could be used as an M-Ary for OFDM system as in section V. The conclusions of this research is given by section VI.

II. RADON TRANSFORM (RT)

Radon transform is used in many branches of science, X-ray crystallography, microwave scattering and others. The medical

Khalid G Samarah is with the Faculty of Engineering, Department of Electrical Engineering, Mu'tah University, Al-Karak, 61710, Jordan, e-mail: kgsamarah@mutah.edu.jo.

computed tomography (CT) has attracted more attention than any other application of the RT. The basic data obtained in a CT procedure are X-ray transmission measurements through a 2D slice of a body. Each measured transmission value is simply related to a line integral of the X-ray attenuation coefficient in this slice [6], in a narrow sense, tomography is the problem of reconstructing the interior of an object by passing radiation through it and recording the resulting intensity over a range of directions.

Fig. 2 illustrates a certain two dimensional object defined by the real function $f(x,y)$ on a certain Cartesian coordinate system. Defining a line $L(\theta,\rho)$ through the object function parameterized by (θ) "the angle between the line and the y-axis" and by (ρ) "the position where this line intersects with the detector line or the displacement of the lines through the object".
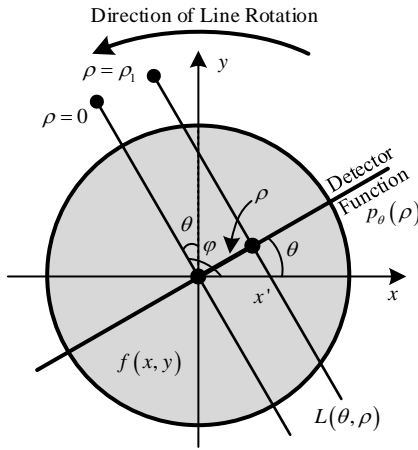

Fig. 2. Radon Transform Demonstration

The line $L(\theta,\rho)$ in this system holds the detector array for a certain projection direction $(0 \leq \theta \leq \pi)$, which is rotated by the angle in the counterclockwise direction relative to the original x-y coordinate system. This gives rise to the attenuated intensity measurement function $I_\theta(\rho)$ for all values of displacement (ρ). The (logarithmic) transformed measurement function $p_\theta(\rho)$, a parallel beam projection, is then computed.

In X-ray transmission it is usually a good approximation to assume that a thin pencil beam of monoenergetic X-rays is attenuated in accordance with Beer-Lambert Law, which states that: the decrease in intensity of light with thickness of the absorbing medium at any point is directly proportional to the intensity of light [21]. For a homogeneous medium of thickness (L), this means that

$$I = I_0 e^{-\mu L} \qquad (2)$$

where (I) is the X-ray flux transmitted through the medium, (I_0), is the flux that would be transmitted in the absence of the medium, and (μ) is the linear attenuation coefficient. For an inhomogeneous medium such as the human body, $\mu = \mu(\mathbf{r})$ is a function of position, and Equation (2) must be replaced with

$$I = I_0 \exp\left(-\int_S^D \mu(\mathbf{r}) dl\right) \qquad (3)$$

where the line integral runs from the source position S to the detector position D. In computed tomography, intensity measurements are made for many line-integral paths confined to a plane, and $(\mathbf{r})$ is therefore a 2D position vector with Cartesian components (x,y). The logarithm of (I/I_0), is linearly related to the line integral:

$$-\ln\left(\frac{I}{I_0}\right) = \int_S^D \mu(\mathbf{r}) dl = p_\theta(\rho) \qquad (4)$$

Radon transform of a real function $f(x,y)$, represents the linear attenuation coefficient of the inhomogeneous medium, is defined on a family of lines, having the value of the line integral along $L(\theta,\rho)$ [5, 22, 23]. On this line, we measure what is called the detector function $p_\theta(\rho)$ or the forward projection. Thus, Radon can be seen as the family of projections, where the projection $p_\theta(\rho)$ is the restriction of Radon transform on the set of all lines parallel to the line containing the origin with direction (θ), $L(\theta,0)$, for different displacements (ρ).

The parallel lines of $L(\theta,0)$ are the lines with a displacement of (ρ), or shifted to the left or to the right on the x-y plane with (x') as shown in Fig. 2, given as follows:

$$L(\theta,\rho) = \{(x,y) \in \mathbb{R} : y = k(x - x') = kx - kx'\} \qquad (5)$$

From Fig. 2, $(k = \tan\varphi)$ is the slope of the line, $\rho = x'\sin\varphi$ and the angle $\left(\varphi = \theta + \dfrac{\pi}{2}\right)$, thus, the parallel line in Equation (5) is given as follows:

$$y = \frac{\sin\varphi}{\cos\varphi} x - \frac{\sin\varphi}{\cos\varphi} \times \frac{\rho}{\sin\varphi}$$

$$y = \frac{\sin\left(\theta + \dfrac{\pi}{2}\right)}{\cos\left(\theta + \dfrac{\pi}{2}\right)} x - \frac{\rho}{\cos\left(\theta + \dfrac{\pi}{2}\right)} \qquad (6)$$

$$y \cos\left(\theta + \frac{\pi}{2}\right) = x \sin\left(\theta + \frac{\pi}{2}\right) - \rho$$

$$-y \sin\theta = x \cos\theta - \rho$$

$$y \sin\theta + x \cos\theta = \rho \qquad (7)$$

This line is then a collection of all the points in the coordinate system and written as follows [4, 6, 19]:

$$L(\theta,\rho) = \{(x,y) \in \mathbb{R} : x \cos\theta + y \sin\theta = \rho\} \qquad (8)$$

The slope of this line is $\left(k = \tan\varphi = \dfrac{\sin(\varphi)}{\cos(\varphi)} = \dfrac{\cos\theta}{-\sin\theta} \right)$, where (θ) is the angle of the displacement (ρ) with the x-axis. For vertical lines, $\left(\varphi = \dfrac{\pi}{2} = \theta + \dfrac{\pi}{2} \right) \Rightarrow \theta = 0$ and for horizontal lines, $\left(\varphi = \pi = \theta + \dfrac{\pi}{2} \right) \Rightarrow \theta = \dfrac{\pi}{2}$, thus Equation (8) is written as follows:

$$L(0,\rho) = \{(x,y) \in \mathbb{R} : x = \rho\}$$
$$L\left(\frac{\pi}{2},\rho\right) = \{(x,y) \in \mathbb{R} : y = \rho\} \qquad (9)$$

Mathematically, the integral of $f(x,y)$ along this line can be obtained by multiplying $f(x,y)$ by the line mass $\delta(x\cos\theta + y\sin\theta - \rho)$, which has support the x-y plane along the line of Equation (8) and then integrating the product function over the x-y plane as follows:

$$p_\theta(\rho) = \int_{-\infty}^{\infty}\int_{-\infty}^{\infty} f(x,y)\delta(x\cos\theta + y\sin\theta - \rho)dxdy \quad (10)$$

At this point, we finally have all that we need to define the measured linear projection data of the function $f(x,y)$ under the annual data and detector position (ρ).
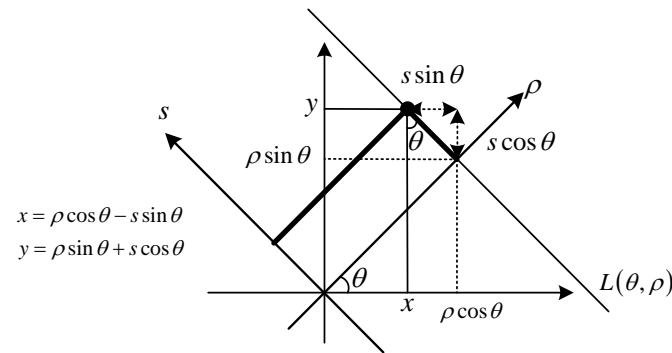

Fig. 3. Coordinates Translation

By using the analysis and conversion of axes as illustrated in Fig. 3, the projection function that represents the straight-line integral of $f(x,y)$ along the line $L(\theta,\rho)$ is written with the change of variables as follows:

$$p_\theta(\rho) = \int_{-\infty}^{\infty} f(\rho\cos\theta - s\sin\theta, \rho\sin\theta + s\cos\theta)ds \quad (11)$$

If we do this for all projection angles and all positions on the detector line so this basically means that we're rotating the detector line around the object function constantly building a detector function each time. Then we end up with the Radon transform.

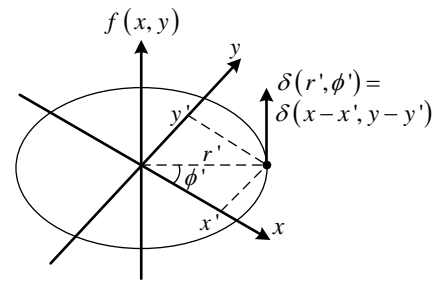$$\mathcal{R}_f(\theta,\rho) = \int_{L(\theta,\rho)} f(x,y)ds \qquad (12)$$

Fig. 4. Example Illustration

To illustrate the two-dimensional nature of the operation defined in Equation (10) the Radon transform of the two-dimensional impulse function $\delta(r',\phi')$ is considered as shown in Fig. 4. Substituting this impulse into the Equation directly yields:

$$\mathcal{R}\{\delta(r',\phi')\} = \mathcal{R}\{\delta(x-x',y-y')\} = p_\theta(\rho)$$
$$= \int_{-\infty}^{\infty}\int_{-\infty}^{\infty} \delta(x-x',y-y')\delta(x\cos\theta + y\sin\theta - \rho)dxdy \quad (13)$$

Using the characteristic of the Dirac function,

$$\int_{-\infty}^{\infty} f(t)\delta(t)dt = f(0)$$
$$\int_{-\infty}^{\infty} f(t)\delta(t-t_0)dt = f(t_0) \qquad (14)$$

$$p_\theta(\rho) = \delta(\rho - x'\cos\theta - y'\sin\theta) \qquad (15)$$

This Equation specifies a line mass supported on the curve $(\rho = x'\cos\theta + y'\sin\theta)$ in the $(\theta\rho - plane)$. From Fig. 4, $(x' = r'\cos\phi')$, $(y' = r'\sin\phi')$ and $(r'^2 = x'^2 + y'^2)$, then the line mass could be written as follows:

$$\rho = x'\cos\theta + y'\sin\theta = r\cos\phi\cos\theta + r\sin\phi\sin\theta$$
$$\rho = \begin{cases} 0.5r\cos(\theta-\phi) + 0.5r\cos(\theta+\phi) + \\ 0.5r\cos(\theta-\phi) - 0.5r\cos(\theta+\phi) \end{cases} \qquad (16)$$
$$\rho = r\cos(\theta-\phi)$$

Equation (15) is then written as:

$$p_\theta(\rho) = \delta(\rho - r\cos(\theta-\phi)) \qquad (17)$$

The Radon transform of the two-dimensional impulse function is more than simply an example of the Radon transform operation. Since an arbitrary function $f(x,y)$ can be expressed as a continuous sum of impulses, i.e.

$$f(x,y) = \int_{-\infty}^{\infty}\int_{-\infty}^{\infty} f(x',y')\delta(x-x',y-y')dx'dy' \quad (18)$$

Since the Radon transform operation is linear, then (by superposition) the Radon transformation of this continuous sum of impulses Equation (18) is a continuous sum of the line masses in Equation (13). Thus, the line mass obtained in Equation (13) is the "point spread function" of the Radon transform operation. Viewing the Radon transform of an arbitrary function $f(x,y)$ as a superposition of these line

masses, supported on sinusoids in the $(\theta\rho - plane)$, provides a simple procedure for obtaining a bound on the effective band region of the Radon transform [i.e., the support of the Fourier transform of $p_\theta(\rho)$.

Since $p_\theta(\rho) = \delta(\rho - r\cos(\theta - \phi))$, the line mass "point spread function" of the Radon transform operation is given by:

$$\rho = r\cos(\theta - \phi). \tag{19}$$

This represents the sinogram resulted from scanning the object $f(x, y)$. For different positions of the Dirac function with the same magnitude (r) and different angles (ϕ), the line mass "point spread function" of the Radon transform operation will results in the sinogram of the cosine function shifted with these angles as shown in Fig. 5. This is a result of scanning the object with different lines parallel to that at the origin with different rotation angles.

With $(\theta = 0)$, the lines are vertically scanning the object. The four lines that can scan the Dirac functions assumed in this

example (see Fig. 5a) are those with the following displacements: $L\left(\frac{-r}{\sqrt{2}}, 0\right)$, $L(0,0)$, $L\left(\frac{r}{\sqrt{2}}, 0\right)$ and $L(r, 0)$. Those lines get the values of the four points shown in Fig. 5 at $(\theta = 0)$. For $\left(\theta = \frac{\pi}{4}\right)$, the lines scan the object at an angle of $\left(\frac{3\pi}{4}\right)$ since $\left(\varphi = \theta + \frac{\pi}{2}\right)$. Fig. 5b illustrates that only three lines can scan the four Dirac functions, where the line with displacement of $\left(\frac{r}{\sqrt{2}}\right)$ scans two Dirac functions as shown in Fig. 5 with the intersection of the two sinusoidal represents the Dirac function in the sinogram.

For all values of $(\theta \, \& \, \rho)$, the result will be a sinusoidal shape for each of the Dirac functions used in the example. Thus, for the whole object $f(x, y)$ $((p \times p)$ Shepp-Logan phantom), a sinogram shape is resulted as shown in Fig. 5.
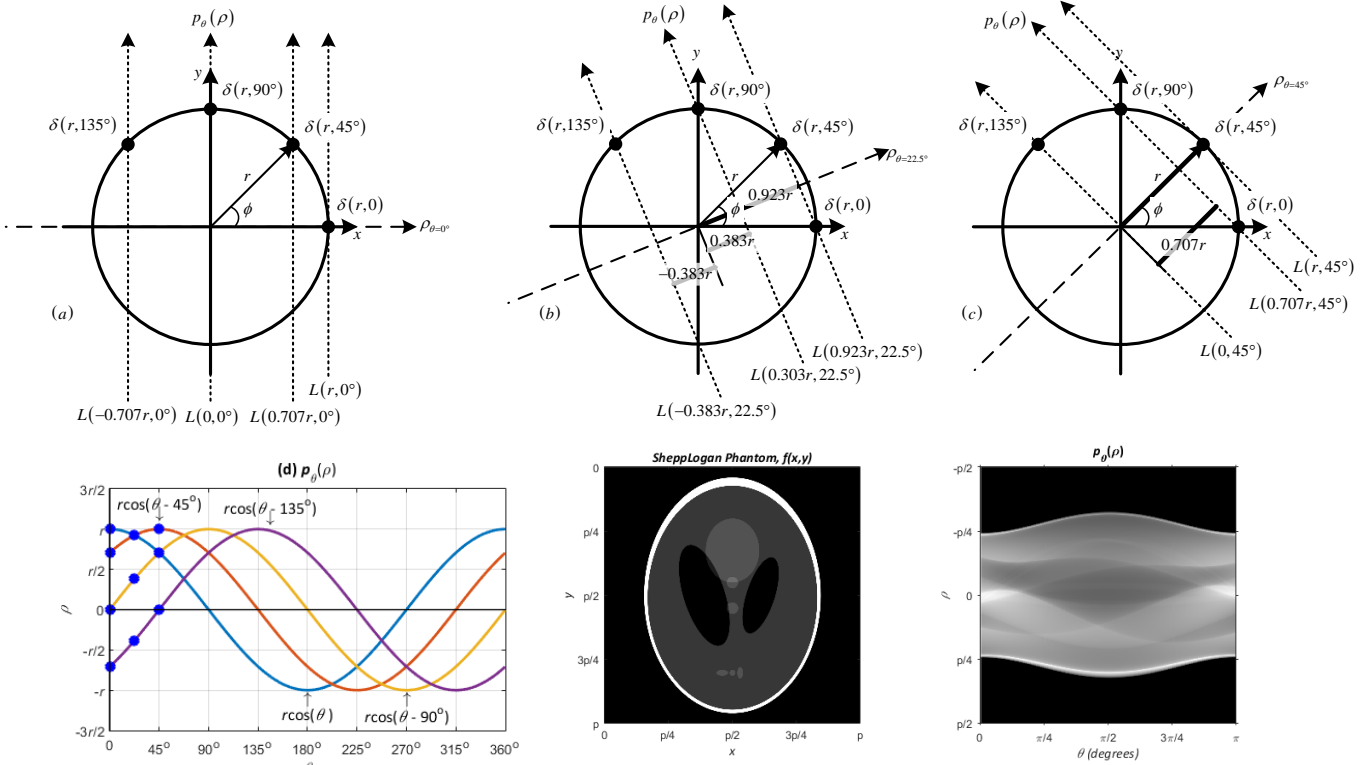

Fig. 5. Rotating $L(\theta, \rho)$ to scan $\delta(r, \emptyset)$ and Line mass "point spread function" for $\emptyset = 0, 45^o, 90^o, 135^o$ and the Sinogram of Shepp-Logan head phantom

III. FOURIER SLICE THEOREM

Analytical reconstruction methods are based on the Fourier slice theory that can be used to build the reconstruction from a projection data. To understand the Fourier slice theorem, some basic knowledge on Fourier analytics is required [24-26].

The Fourier Slice theorem states that: a one dimensional Fourier transform of the (projection) detector function $p_\theta(t)$ at an angle (θ) is exactly the same as a (slice) line through the

two dimensional Fourier representation of the entire object even more it is aligned to the origin at the exact angle (θ), [27-29] Fig. 6.

(The Fourier Slice Theorem also known tensor transform-based algorithm of the N×N-point 2-D DFT, which was developed not only for prime N, and for other cases of N, as well [30]). A given two-dimensional object function $f(x, y)$ represented on a Cartesian domain is shown in Fig. 6.

The Fourier representation is given by taking the 2D-Fourier transform of the unknown object function. The only known its detector functions for a set of different angles.

By measuring a single projection of an object, we are able to fill in a single line in the Fourier domain (red or blue lines). Obviously as we then acquire projections from multiple angles, we can then essentially construct the full Fourier representation of that object.

Then a two-dimensional inverse Fourier transform can be applied on that data to retrieve or to reconstruct the original object function. The 2D FT is given as follows:

$$\mathcal{F}_{2D}\{f(x,y)\} = F(u,v) = \int_{-\infty}^{\infty}\int_{-\infty}^{\infty} f(x,y)e^{-j2\pi(ux+vy)}dxdy \quad (20)$$
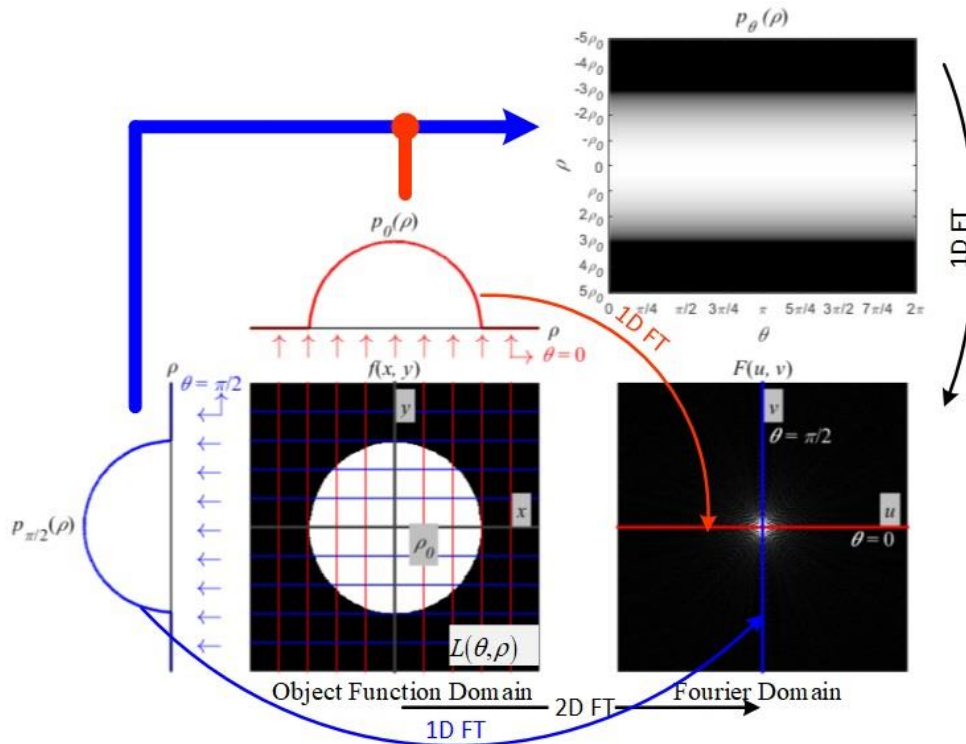

Fig. 6. Projection and the 2D-FT and Fourier Slice Theorem (Forward)

The 1D FT of the radon transform is given as follows:

$$P_\theta(\omega) = \int_{-\infty}^{\infty} p_\theta(\rho)e^{-j2\pi\omega\rho}d\rho \quad (21)$$

Using Equation (10),

$$P_\theta(\omega) = \int_{-\infty}^{\infty}\int_{-\infty}^{\infty} f(x,y)dxdy\int_{-\infty}^{\infty} \delta(x\cos\theta + y\sin\theta - \rho)e^{-j2\pi\omega\rho}d\rho$$
$$(22)$$

From the characteristics of the Dirac function,

$$\int_{-\infty}^{\infty} \delta(x\cos\theta + y\sin\theta - \rho)e^{-j2\pi\omega\rho}d\rho = e^{-j2\pi\omega(x\cos\theta + y\sin\theta)} \quad (23)$$

Thus, Equation (22) is as follows:

$$P_\theta(\omega) = \int_{-\infty}^{\infty}\int_{-\infty}^{\infty} f(x,y)e^{-j2\pi\omega(x\cos\theta + y\sin\theta)}dxdy$$
$$P_\theta(\omega) = \int_{-\infty}^{\infty}\int_{-\infty}^{\infty} f(x,y)e^{-j2\pi x\omega\cos\theta}e^{-j2\pi y\omega\sin\theta}dxdy \quad (24)$$
$$P_\theta(\omega) = F(\omega\cos\theta, \omega\sin\theta)$$

Comparing Equation (24) with Equation (20) given that $u = \omega\cos\theta$, and $v = \omega\sin\theta$, which proves the Fourier Slice

Theorem, where the 1D Fourier transform of the radon transform (the projection function) is the 2D Fourier transform of the object function as follows:

$$\mathcal{F}_{1D}\{p_\theta(\rho)\} = P_\theta(\omega) = \mathcal{F}_{2D}\{f(x,y)\} = F(u,v) \quad (25)$$

Using the Fourier transform, we can find the Radon transform of the object function by doing the 2D Fourier transform followed by the inverse 1D Fourier transform shown in Equation (1) and given as follows:

$$\mathcal{R}\{f(x,y)\} = \mathcal{F}_{1D}^{-1}\{\mathcal{F}_{2D}\{f(x,y)\}\} \quad (26)$$

To reconstruct the object function using the Fourier slice theorem, an inverse operation is done as follows:

$$f(x,y) = \mathcal{F}_{2D}^{-1}\{\mathcal{F}_{1D}\{p_\theta(\rho)\}\} = \mathcal{F}_{2D}^{-1}\{\mathcal{F}_{1D}\{\mathcal{R}\{f(x,y)\}\}\}$$
$$(27)$$

The problem of this approach is that the amount of measurements in practice is finite, which leads to a Fourier domain that is sampled in a difficult way to work with. Free samples lie in circles rather than on a square grid as shown in

Fig. 7, which is required for practical algorithms that perform the inverse transformation such as the fast Fourier transform.

This needs to apply interpolation in the Fourier domain, which is not acceptable. In the other hand, the sampling distribution of the Fourier domain is much denser near the origin than it is for the outer regions; this means that for the lowest frequencies there is many data available meaning that these low frequencies will be reconstructed accurately.

The high frequencies however, which is where most of the finer details of the object are located are not that greatly sampled and will not be accurately reconstructed after the inverse Fourier transform and this will lead to very blurry images. Even though you cannot use the Fourier slice theorem to directly create reconstructions it does form the basis for another reconstruction methods called filtered back-projection, which cleverly manages to overcome the problems of the Fourier Slice Theorem by introducing an additional filtering phase and by replacing the inverse Fourier transform with a different operation [31, 32].

IV. THE FINITE RADON TRANSFORM (FRAT)

The Finite Radon Transform (FRAT) has been discussed in many research papers and defined for 2-D images. It is a DRT that is defined on the same finite geometry as the Discrete Fourier Transform (DFT) [33-35].
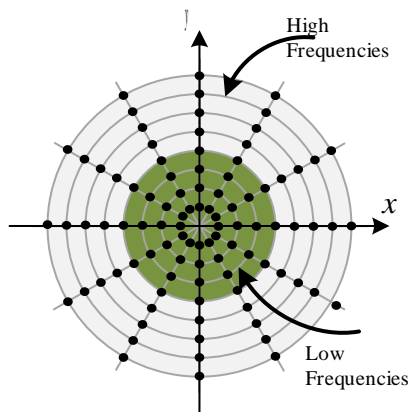
Fourier Sampling with Fourier Slice Theorem
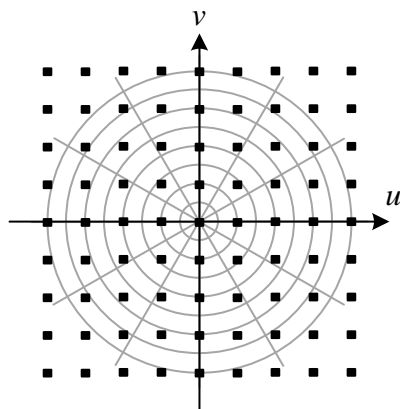
Sampling Required by Fast Fourier Transform

Fig. 7. Sampling in the Fourier Domain

During the last decade, elements of a finite Radon transform theory have appeared mainly in the field of combinatorics. The fundamental concept due to Bolker is as follows: The finite Radon transform of a real function (f) defined on a finite set (X) (with respect to a collection (Y) of its subsets: blocks) is the function $(\hat{f})$ on (Y), the values of which are obtained by summing (f) over these subsets: blocks. It seems quite impossible to say anything about this transform without additional conditions on the collection (f), however, when considered on special combinatorial or algebraical structures like designs, metroid's, lattices, groups, etc., [36-38].

Matus and Flusser [39] presented a model of FRAT that generalizes to finite group projections in the traditional RT theory applied to square array of prime sizes $p \times p$. The Radon projector averages a function on a group over normalizing of a subgroup. Deriving reconstruction formulae, which were formally similar to the convolved back projection ones and an iterative reconstruction technique is found to converge after finite number of steps, consequently, it may be exactly inverted via the Fast Fourier Transform (FFT) without any filtering or interpolation. The Finite Radon transform (FRAT) is defined as the summation of image pixels over a certain set of lines [1, 12, 39, 40].

Another technique applied to dyadic square arrays $2^n \times 2^n$ called the DPRT "Discrete periodic RT" [15]. This technique is developed to prime-adic arrays $p^n \times p^n$. Later on a generalized FRAT that is applied to square arrays of arbitrary size $N \times N$ and based on a modulo arithmetic is proposed by [41], where the operation of generalized FRAT made it useful imaging tool that reduced 2D problems to a set of 1D problem.

Most of the radon transforms were not designed to be invertible transforms for digital images. Alternatively, the FRAT, which means transform for finite length signals, provides an interesting solution.

A group is called finite, if it contains finitely many elements, i.e., $\{0,1,...,p-1\}$ is called the group of integers modulo p (Z_p). The number of elements in the finite group is called its order [12].

Do and Vetterli defined FRAT as the summation of image pixels $f[i,j]$, over some set of lines $L_{k,l}$, which is a set of line points on (Z_p^2). Denote $Z_p = \{0, 1, ..., p-1\}$ as a finite field with modulo p operations, where p is a prime number [1, 39]. The FRAT of a real function (f) over (Z_p^2) is given as follows:

$$r_k[l] = FRAT_f[k,l] = \frac{1}{\sqrt{p}} \sum_{(i,j) \in L_{k,l}} f[i,j] \qquad (28)$$

$(L_{k,l})$ is a set of line points on (Z_p^2) that is presented by the slope or direction $k \in Z_p^* = \{0, 1, ..., p\}$ and intercept $l \in Z_p = \{0, 1, ..., p-1\}$, where:

$$L_{k,l} = \{(i,j): j = ki + l \ (\text{mod } p), \ i \in Z_p\}$$
$$L_{p,l} = \{(l,j): i = l, \qquad\qquad j \in Z_p\} \qquad (29)$$

When the slope is zero (horizontal lines), the line equation will be $(j = l \ for \ all \ i \in Z_p)$. In addition, when the slope is infinity (vertical lines), the line equation will be $(i = l \ for \ all \ j \in Z_p)$. For slopes between zero and infinity, Equation (29) is valid [1, 39, 42]. The FRAT of a real function is then given as follows:

$$r_k[l] = \frac{1}{\sqrt{p}} \sum_{i=0}^{p-1} f[i, \ ki + l \ (\text{mod } p)]$$
$$r_p[l] = \frac{1}{\sqrt{p}} \sum_{j=0}^{p-1} f[l, j] \qquad (30)$$

For compacting energy, it is better to subtract the mean from the image $f[i,j]$ before transforming it. On the other hand, the $l_2 - norm$ (known as the Euclidean norm, which calculates the distance of the vector coordinate from the origin of the vector space) is normalized by introducing the factor $\left(1/\sqrt{p}\right)$.

For each image, there are $(p+1)$ directions and (p) intercepts that obviously, there are $p(p+1)$ number of lines and every line contains (p) number of points. These represent $(p-1)$ coefficients at $(p+1)$ directions in addition to the mean value, which make up $(p-1)(p+1)+1 = p^2$ FRAT coefficients in the FRAT domain [1]. This indicates that the function contains (p^2) points input to the FRAT and $p(p+1)$ number of output points resulted from integrating this number of lines. For general definition of lines in (Z_p^2) plane:

$$L_{a,b,t}' = \{(i,j) \in Z_p^2: \ ai + bj - t = 0 \ (\text{mod } p)\} \qquad (31)$$

where $(a,b,t) \in Z_p$ and $(a,b) \neq 0$. For the finite line $(L_{a,b,t}')$, (a,b) has the role of a normal vector, (t) is the translation parameter. This is by analogy with the line Equation (8) $L(\theta, \rho) = \{(x,y) \in \mathbb{R} : x\cos\theta + y\sin\theta = \rho\}$. Since the line slope represents $(k = \tan\varphi)$ as in Fig. 2 above, and

$$\left[\cos(\varphi) = \cos\left(\theta + \frac{\pi}{2}\right) = -\sin\theta\right] \qquad \text{and}$$

$$\left[\sin(\varphi) = \sin\left(\theta + \frac{\pi}{2}\right) = \cos\theta\right], \text{ thus the slope is given as:}$$

$$k = \frac{\sin\varphi}{\cos\varphi} = \frac{\cos\theta}{-\sin\theta} \qquad (32)$$

For fixed normal vector (a,b), $\{L_{a,b,t}' : t \in Z_p\}$ is a set of lines in the (Z_p^2) plane. This set is equal to the set of p lines $\{L_{k,l} : l \in Z_p\}$ with the same slope k that is:

$$L_{k,l} = \{(i,j): j = ki + l \ (\text{mod } p), \ i \in Z_p\}$$
$$L_{p,l} = \{(l,j): i = l, \qquad\qquad j \in Z_p\}$$
$$L_{a,b,t}' = \{(i,j) \in Z_p^2: \ ai + bj - t = 0 \ (\text{mod } p)\}$$
$$j = ki + l = -ab^{-1}i + b^{-1}t$$
$$-ab^{-1}i = ki \Rightarrow k = \frac{a}{-b} \qquad (33)$$
$$b^{-1}t = l \Rightarrow l = \frac{t}{b}$$
$$L_{a,b,t}' \equiv L_{k,l} \ \text{ if } \ k = \frac{-a}{b}, \ b \neq 0, \ l = \frac{t}{b}$$

And as in [42],

$$L_{k,l} = \{(i,j): j = ki + l \ (\text{mod } p), \ i \in Z_p\}$$
$$L_{p,l} = \{(l,j): i = l, \qquad\qquad j \in Z_p\}$$
$$L_{a,b,t}' = \{(i,j) \in Z_p^2: \ ai + bj - t = 0 \ (\text{mod } p)\} \qquad (34)$$
$$i = l = \frac{t}{a}, \ L_{a,b,t}' \equiv L_{p,l} \ \text{ if } \ a \neq 0, \ b = 0, \ l = \frac{t}{a}$$

The FRAT could be written as follows:

$$r_{a,b}[t] = FRAT_f(a,b,t) = \frac{1}{\sqrt{p}} \sum_{(i,j) \in L_{a,b,t}} f[i,j] \qquad (35)$$

For this equation, the FRAT projection sequence $(r_{a,b}[0], \ r_{a,b}[1], ..., \ r_{a,b}[p-1])$ is simply a reordering of the FRAT sequence $(r_k[0], \ r_k[1], ..., \ r_k[p-1])$. The normal vector (a,b) controls the ordering of these coefficients in each FRAT projection as well as the represented direction of those projections. $r_k[l]$ uses the set of $(p+1)$ normal vectors $(\boldsymbol{u}_k)$ where:

$$\boldsymbol{u}_k = (-k,1) \quad k = 0, \ 1, ..., \ p-1, \ and \ \boldsymbol{u}_p = (1,0) \qquad (36)$$

To represent $r_{a,b}[k]$, we need normal vector $\{(a_k, b_k): k \in Z_p^*\}$ to cover all $(\boldsymbol{u}_k \ \& \boldsymbol{u}_p)$ normal vectors. In addition, the set of lines with normal vectors (a,b) equals to the set of lines with normal vectors (na, nb), the $(p-1)$ choices are given as follows:

$$(a_k, b_k) = n\boldsymbol{u}_k \ \ where \ n = 1, \ 2, ..., \ p-1$$
$$(a_0, b_0) = (0,1) \ \& \ (a_p, b_p) = \boldsymbol{u}_p = (1,0) \qquad (37)$$

The good choice of the $(p+1)$ normal vectors is resulted from the Discrete Projection –Slice Theorem, which shows that: The 1D DFT $R_{a,b}[\omega]$ of a FRAT projection $r_{a,b}[t]$ is identical

to the 2D DFT $F[u,v]$ of $f[i,j]$ evaluated along a discrete slice through the origin at direction (a,b):

$$R_{a,b}[\omega] = \mathcal{F}_{1D}\{r_{a,b}[t]\} = \sum_{t=0}^{p-1} r_{a,b}[t] e^{-j2\pi\frac{\omega t}{p}}$$
$$= \sum_{t=0}^{p-1}\left(\frac{1}{\sqrt{p}}\sum_{(i,j)\in L_{a,b,t}} f[i,j]\right) e^{-j2\pi\frac{\omega t}{p}} \quad (38)$$
$$= \frac{1}{\sqrt{p}}\sum_{i=0}^{p-1}\sum_{j=0}^{p-1} f[i,j] e^{-j2\pi\frac{\omega(ai+bj)}{p}}$$
$$R_{a,b}[\omega] = F[a\omega,b\omega] = \mathcal{F}_{2D}\{f[i,j]\} = F[u,v]$$

This shows the influence of the normal vectors (a,b) that control the order of the coefficients in the Fourier slices (also known tensor transform-based algorithm of the N ×N-point 2D DFT, which was developed not only for prime N, and for other cases of N, as well [30]). In particular, $F(a,b)$ represents the first harmonic of the FRAT projection. Since most of the interested types of images, the energy in concentrated in the low frequency, the represented normal vectors (a,b) should be chosen to be as close to the origin of the Fourier plane as possible. This lead to define the set of $(p+1)$ optimal normal vectors $\{(a_k^*,b_k^*):k\in Z_p^*\}$ as follows [1, 40]:

$$(a_k^*,b_k^*) = \arg\min_{\substack{(a_k,b_k)\in\{nu_k:\,1\leq n\leq p-1\}\\C_p(b_k)\geq 0}}\left\|\left(C_p(a_k),C_p(b_k)\right)\right\| \quad (39)$$

A. Optimal Normal Vectors

From Equation (39), the new optimal normal vectors are obtained as follows:

- $(a_k,b_k) \in \{nu_k : 1\leq n\leq p-1\}$ are the points on the periodic Fourier plane
- Taking into account that $(a_0,b_0)=(0,1)$ & $(a_p,b_p)=(1,0)$ are the vertical and horizontal slices in the Fourier domain, the number of slices in the Fourier domain are $(p-1)$ slices distributed around the origin where $k=\left[\frac{-(p-1)}{2}:-1,\ 1:\frac{p-1}{2}\right]$

$$a_k = -nk$$
$$a_k = \begin{bmatrix} -1 \\ -2 \\ \vdots \\ -(p-1) \end{bmatrix}\begin{bmatrix} \frac{-(p-1)}{2} & .. & -1 & 1 & .. & \frac{p-1}{2} \end{bmatrix} \quad (40)$$

$$a_k = \begin{bmatrix} \frac{(p-1)}{2} & .. & 1 & -1 & .. & \frac{-(p-1)}{2} \\ \frac{2(p-1)}{2} & .. & 2 & -2 & .. & \frac{-2(p-1)}{2} \\ \vdots & \vdots & \vdots & \vdots & \vdots & \vdots \\ \frac{(p-1)^2}{2} & .. & p-1 & -(p-1) & .. & \frac{-(p-1)^2}{2} \end{bmatrix} \quad (41)$$

- The other element of the normal vectors is (b_k), which has the values of (n) for each group of (a_k) values as follows:

$$b_k = n\times 1_k$$
$$b_k = \begin{bmatrix} 1 \\ 2 \\ \vdots \\ p-1 \end{bmatrix}\begin{bmatrix} 1 & \dots & 1 & 1 & \dots & 1 \end{bmatrix} \quad (42)$$

$$b_k = \begin{bmatrix} 1 & \dots & 1 & 1 & \dots & 1 \\ 2 & \dots & 1 & 2 & \dots & 2 \\ \vdots & \vdots & \vdots & \vdots & \vdots & \vdots \\ p-1 & \dots & p-1 & p-1 & \dots & p-1 \end{bmatrix} \quad (43)$$

- for example, if $(p=5)$, then

$$(a_k,b_k)_{p=3} = \begin{bmatrix} (1,1) & (-1,1) \\ (2,2) & (-2,2) \end{bmatrix}$$
$$(a_k,b_k)_{p=5} = \begin{bmatrix} (2,1) & (1,1) & (-1,1) & (-2,1) \\ (4,2) & (2,2) & (-2,2) & (-4,2) \\ (6,3) & (3,3) & (-3,3) & (-6,3) \\ (8,4) & (4,4) & (-4,4) & (-8,4) \end{bmatrix} \quad (44)$$

- $C_p(x) = x - p\cdot round\left(\frac{x}{p}\right)$ is the centralized function of period p applied to (a_k,b_k) as follows:

$$C_3(a_k,b_k) = (a_k,b_k) - 3\times round\left(\frac{(a_k,b_k)}{3}\right)$$
$$C_5(a_k,b_k) = (a_k,b_k) - 5\times round\left(\frac{(a_k,b_k)}{5}\right) \quad (45)$$

$$C_3(a_k,b_k) = \begin{bmatrix} (1,1) & (-1,1) \\ (-1,-1) & (1,-1) \end{bmatrix}$$
$$C_5(a_k,b_k) = \begin{bmatrix} (2,1) & (1,1) & (-1,1) & (-2,1) \\ (-1,2) & (2,2) & (-2,2) & (1,2) \\ (1,-2) & (-2,-2) & (2,-2) & (-1,-2) \\ (-2,-1) & (-1,-1) & (1,-1) & (2,-1) \end{bmatrix} \quad (46)$$

- imposed to remove ambiguity of choosing between (a,b) & $(-a,-b)$, this is done by eliminating points with negative angle. Thus, the optimal normal vectors have angles between $(0,\pi)$, thus all negative b_k values represent negative angles.

$$C_3\left(a_k,b_k\right)_{C_p(b_k)\geq 0} = \begin{bmatrix} (1,1) & (-1,1) \\ NaN & NaN \end{bmatrix} \qquad (47)$$

$$C_5\left(a_k,b_k\right)_{C_p(b_k)\geq 0} = \begin{bmatrix} (2,1) & (1,1) & (-1,1) & (-2,1) \\ (-1,2) & (2,2) & (-2,2) & (1,2) \\ NaN & NaN & NaN & NaN \\ NaN & NaN & NaN & NaN \end{bmatrix} \qquad (48)$$

- Minimization is done for each $k \in Z_p^*$ by computing $(p-1)$ distances and select the smallest one. If the distances are equal, the minimum angle is chosen. $\left\|\left(C_p\left(a_k\right),C_p\left(b_k\right)\right)\right\|$ is the distance from the origin to the point $\left(a_k,b_k\right)$ on the periodic Fourier plane (Euclidean norm).

$$\left|C_3\left(a_k,b_k\right)_{C_p(b_k)\geq 0}\right| = \begin{bmatrix} \boxed{\sqrt{2}} & \boxed{\sqrt{2}} \\ NaN & NaN \end{bmatrix}$$

$$\angle\theta_3 = \begin{bmatrix} \angle 45° & \angle 135° \\ NaN & NaN \end{bmatrix} \qquad (49)$$

$$\left|C_5\left(a_k,b_k\right)_{C_p(b_k)\geq 0}\right| = \begin{bmatrix} \sqrt{5} & \boxed{\sqrt{2}} & \boxed{\sqrt{2}} & \sqrt{5} \\ \boxed{\sqrt{5}} & \sqrt{8} & \sqrt{8} & \boxed{\sqrt{5}} \\ NaN & NaN & NaN & NaN \\ NaN & NaN & NaN & NaN \end{bmatrix}$$

$$\angle\theta_5 = \begin{bmatrix} \angle 26.565° & \angle 45° & \angle 135° & \angle 153.435° \\ \angle 116.565° & \angle 45° & \angle 135° & \angle 63.435° \\ NaN & NaN & NaN & NaN \\ NaN & NaN & NaN & NaN \end{bmatrix} \qquad (50)$$

- The minimum distances and there positions are given as follows:

$$\min\{|\mathbf{C}|\}_3 = \begin{bmatrix} 1.4142 & 1.4142 \end{bmatrix}$$
$$index_3 = \arg\min\{|\mathbf{C}|\} = \begin{bmatrix} 1 & 3 \end{bmatrix}$$

$$\min\{|\mathbf{C}|\}_5 = \begin{bmatrix} 2.2361 & 1.4142 & 1.4142 & 2.2361 \end{bmatrix}$$
$$index_5 = \arg\min\{|\mathbf{C}|\} = \begin{bmatrix} 2 & 5 & 9 & 14 \end{bmatrix} \qquad (51)$$

- Retrieve $M_0 = \left(a_k^*,b_k^*\right)'$ points and put them in a set of directions, as follows:

$$M_0^3 = C_p\left(a_k,b_k\right)(index) = C_p\left(a_k,b_k\right)(1\ \ 3)$$
$$M_0^3 = \begin{bmatrix} (1,1) & (-1,1) \end{bmatrix}$$

$$M_0^5 = C_p\left(a_k,b_k\right)(index) = C_p\left(a_k,b_k\right)(2\ \ 5\ \ 9\ \ 14)$$
$$M_0^5 = \begin{bmatrix} (-1,2) & (1,1) & (-1,1) & (1,2) \end{bmatrix} \qquad (52)$$

- Adding the vertical and horizontal slices as follows:

$$M_0^3 = \begin{bmatrix} (1,1) & (-1,1) & (1,0) & (0,1) \end{bmatrix}$$
$$\angle\theta_0^3 = \begin{bmatrix} 45° & 135° & 0° & 90° \end{bmatrix}$$

$$M_0^5 = \begin{bmatrix} (-1,2) & (1,1) & (-1,1) & (1,2) & (1,0) & (0,1) \end{bmatrix}$$
$$\angle\theta_0^5 = \begin{bmatrix} 45° & 63.435° & 116.565° & 135° & 0° & 90° \end{bmatrix} \qquad (53)$$

- Sort those directions in ascending order of angles results in the optimal ordering $\left(a_k^*,b_k^*\right)$ as follows:

$$\left(a_k^*,b_k^*\right)_3 = M_0^3 = \begin{bmatrix} (1,0) & (1,1) & (0,1) & (-1,1) \end{bmatrix}$$
$$\left(a_k^*,b_k^*\right)_5 = M_0^5 = \begin{bmatrix} (1,0) & (1,1) & (1,2) & (0,1) & (-1,2) & (-1,1) \end{bmatrix} \qquad (54)$$

After obtaining $\left(a_k^*,b_k^*\right)$, FRAT and its inverse can be computed, where $\left(u_k\ \&\ u_p\right)$ are translated to $\left(a_k^*,b_k^*\right)$, which provides a much more uniform angular coverage as illustrated in Fig. 8.
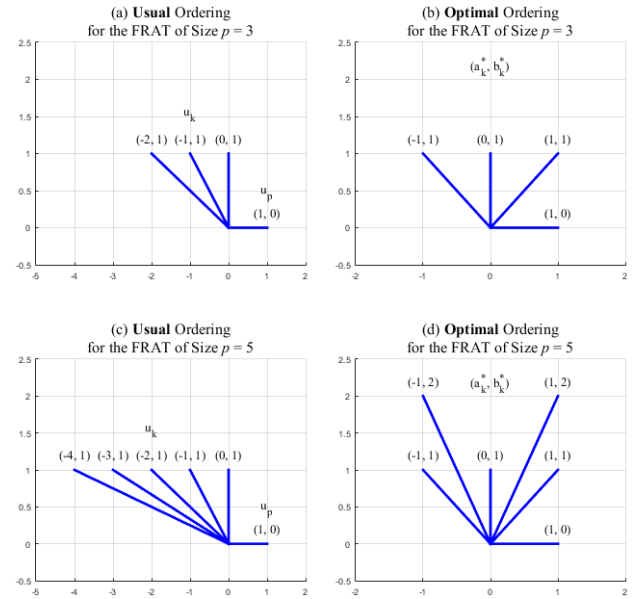

Fig. 8. The Set of Normal Vectors, which Indicate the Represented Directions for $p = 3$ & 5

The normal vectors $\left(a_k^*,b_k^*\right)$ are used to rearrange the 2D Fourier transform data, the inverse 1D Fourier transform is then applied to get the RT of the real function $f(i,j)$.

B. FRAT of Data Input

The input to the FRAT transformation is a $[p \times p]$ matrix represents the image pixels or the real function $f(i,j)$ as shown in Fig. 9, where, p is a prime number [1, 43, 44]. This matrix is 2-D Fourier transformed as follows:

$$F[u,v] = \frac{1}{\sqrt{p}} \sum_{i=0}^{p-1}\sum_{j=0}^{p-1} f[i,j] e^{-j2\pi\frac{ui+vi}{p}}$$

$$where \begin{cases} u = 0 : p-1 \\ v = 0 : p-1 \end{cases} \tag{55}$$
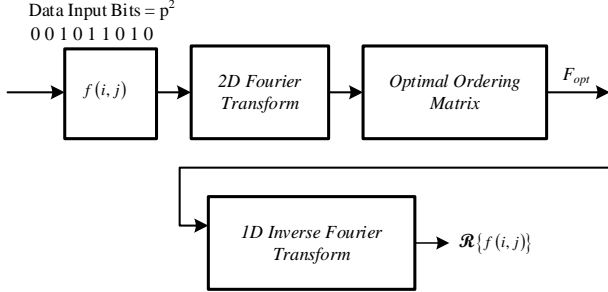
Data Input Bits = p²
0 0 1 0 1 1 0 1 0

Fig. 9. Data Symbols Generation using FRAT

As an example, assume an input frame data number of $p^2 = 9$, where this input is to be arranged in a matrix of $[p \times p] = [3 \times 3]$.

$$0\,0\,1\,0\,1\,1\,0\,1\,0 \Rightarrow f(i,j) = \begin{bmatrix} 0 & 0 & 0 \\ 0 & 1 & 1 \\ 1 & 1 & 0 \end{bmatrix}$$

$$F[u,v] = \frac{1}{\sqrt{3}} \sum_{i=0}^{2}\sum_{j=0}^{2} f[i,j] e^{-j2\pi\frac{ui+vi}{3}} \ where \begin{cases} u = 0:2 \\ v = 0:2 \end{cases} \tag{56}$$

$$F[u,v] = \mathcal{F}_{2D}\{f[i,j]\}$$
$$= \begin{bmatrix} 2.31 & -2.89-0.5i & -2.89+0.5i \\ -1.155 & 0.577+1.0i & -0.289+0.5i \\ -1.155 & -0.289-0.5i & 0.577-1.0i \end{bmatrix} \tag{57}$$

The optimal ordering of $F[u,v]$ matrix as suggested by [1] is started by finding the best directory (normal vectors) of the matrix of $[p \times p] = [3 \times 3]$, which is found to be a $[2 \times (p+1)] = [2 \times 4]$ matrix as follows:

$$\left(a_k^*, b_k^*\right) = \begin{bmatrix} 1 & 1 & 0 & -1 \\ 0 & 1 & 1 & 1 \end{bmatrix} \tag{58}$$

The optimal ordering is related to the (modulo operation) between the normal vectors and coordinates of the Fourier slices $\left(a_k^*, b_k^*\right)$ as follows:

$$U = u' \times a_k^* \bmod p$$
$$V = v' \times b_k^* \bmod p \tag{59}$$

where $(u'\ v')$ are the column vectors of the Fourier slice coordinates, U and V are the Fourier slices used to identify the reordering of the Fourier matrix, thus U and V are given by:

$$U = \begin{bmatrix} 0 & 0 & 0 & 0 \\ 1 & 1 & 0 & 2 \\ 2 & 2 & 0 & 1 \end{bmatrix}, \quad V = \begin{bmatrix} 0 & 0 & 0 & 0 \\ 0 & 1 & 1 & 1 \\ 0 & 2 & 2 & 2 \end{bmatrix} \tag{60}$$

The new optimal ordering matrix $\left(F_{opt}\right)$, which has a dimension of $[p \times (p+1)]$ (Fourier transform of FRAT projections) is given as by the following ordering [1]:

$$UV = 1 + U + p \times V$$

$$UV = 1 + \begin{bmatrix} 0 & 0 & 0 & 0 \\ 1 & 1 & 0 & 2 \\ 2 & 2 & 0 & 1 \end{bmatrix} + 3 \times \begin{bmatrix} 0 & 0 & 0 & 0 \\ 0 & 1 & 1 & 1 \\ 0 & 2 & 2 & 2 \end{bmatrix} \tag{61}$$

$$UV = \begin{bmatrix} 1 & 1 & 1 & 1 \\ 2 & 5 & 4 & 6 \\ 3 & 9 & 7 & 8 \end{bmatrix}$$

$$F_{opt} = F(UV)$$

$$F_{opt} = F\begin{pmatrix} 1 & 1 & 1 & 1 \\ 2 & 5 & 4 & 6 \\ 3 & 9 & 7 & 8 \end{pmatrix}$$

$$F_{opt} = \begin{bmatrix} 2.31 & 2.31 & 2.31 & 2.31 \\ -1.155 & 0.577+1.0i & -2.89-0.5i & -0.289-0.5i \\ -1.155 & 0.577-1.0i & -2.89+0.5i & -0.289+0.5i \end{bmatrix} \tag{62}$$

Take the 1D-IFFT for each column of the matrix $\left(F_{opt}\right)$ to obtain the matrix of Radon coefficients, R and then construct the complex matrix R from the real matrix R to be the data sub-carriers input to the IFFT of the OFDM system. The 1D-IFFT for each column of the matrix $\left(F_{opt}\right)$ is given by:

$$\mathcal{R}\{f(i,j)\} = \mathcal{F}_{1D}^{-1}\{F_{opt}\}$$
$$\mathcal{R}\{f(i,j)\} = \begin{bmatrix} 0 & 1.155 & 0.577 & 0.577 \\ 1.155 & 0 & 1.155 & 1.155 \\ 1.155 & 1.155 & 0.577 & 0.577 \end{bmatrix} \tag{63}$$

C. Inverse FRAT

To reconstruct the object function using the Fourier slice theorem, an inverse operation is done as show in Equation (27) above and rewritten as follows:

$$f(i,j) = \mathcal{F}_{2D}^{-1}\left\{\mathcal{F}_{1D}\{\mathcal{R}\{f(i,j)\}\}\right\} \tag{64}$$

$$\mathcal{F}_{1D}\{\mathcal{R}\{f(i,j)\}\} =$$
$$\mathcal{F}_{1D}\left\{\begin{bmatrix} 0 & 1.155 & 0.577 & 0.577 \\ 1.155 & 0 & 1.155 & 1.155 \\ 1.155 & 1.155 & 0.577 & 0.577 \end{bmatrix}\right\} = F_{opt}$$

$$F_{opt} = \begin{bmatrix} 2.31 & 2.31 & 2.31 & 2.31 \\ -1.155 & 0.577+1.0i & -2.89-0.5i & -0.289-0.5i \\ -1.155 & 0.577-1.0i & -2.89+0.5i & -0.289+0.5i \end{bmatrix} \tag{65}$$

Reorder the optimal matrix using the same normal vectors and optimal ordering used in the FRAT transformation as follows:

$$F_{UV}\begin{pmatrix} 1 & 1 & 1 & 1 \\ 2 & 5 & 4 & 6 \\ 3 & 9 & 7 & 8 \end{pmatrix} = F_{opt}$$

$$F(UV) = \begin{bmatrix} 2.31 & -2.89-0.5i & -2.89+0.5i \\ -1.155 & 0.577+1.0i & -0.289+0.5i \\ -1.155 & -0.289-0.5i & 0.577-1.0i \end{bmatrix} \quad (66)$$

Taking the inverse 2D Fourier Transform results in the following:

$$f(i,j) =$$
$$\mathcal{F}_{2D}^{-1}\left\{ \begin{bmatrix} 2.31 & -2.89-0.5i & -2.89+0.5i \\ -1.155 & 0.577+1.0i & -0.289+0.5i \\ -1.155 & -0.289-0.5i & 0.577-1.0i \end{bmatrix} \right\} \quad (67)$$

$$f(i,j) = \begin{bmatrix} 0 & 0 & 0 \\ 0 & 1 & 1 \\ 1 & 1 & 0 \end{bmatrix}$$

V. M-ARY TECHNIQUE & SIGNAL CONSTELLATION

Construct complex data from the matrix in Equation (63) done by taking the odd columns as real part and the even columns as the imaginary part of the data subcarriers, which are used as an input to the OFDM symbol generator (inverse Fourier transform), this is done by converting the complex matrix into complex column vector as follows:

$$R_{complex} = \begin{bmatrix} 0.577 & 0.577+1.154i \\ 1.154+1.154i & 0.577 \\ 0.577+1.154i & 1.154+1.154i \end{bmatrix} \quad (68)$$

$$Data\ Subcarriers = \begin{bmatrix} 0.577 \\ 1.154+1.154i \\ 0.577+1.154i \\ 0.577+1.154i \\ 0.577 \\ 1.154+1.154i \end{bmatrix} \quad (69)$$

An observation of the output is that it equals to a frame of length $p \times (p+1)/2 = 3 \times 2 = 6$ and the input as mentioned before equals to a frame of length $p \times p = 3 \times 3 = 9$. Focusing on the input number of bits and the output number of symbols, give that always the ratio is constant as follows:

$$Ratio = \frac{in}{out} = \frac{p^2}{p(p+1)/2} = \frac{2p}{p+1} < 2$$
$$\begin{array}{ccccc} p & 3 & 7 & 11 & 37 \\ Ratio & 1.5 & 1.75 & 1.833 & 1.947 \end{array} \quad (70)$$

An observation of the output is that it equals to a frame of length $p \times (p+1)/2$ and the input as mentioned before equals to a frame of length $p \times p$. This leads to a ratio between the input and the output as follows:

$$Ratio = \frac{in}{out} = \frac{p^2}{p(p+1)/2} = \frac{2p}{p+1} < 2 \quad (71)$$

This ratio ensures that the data rate will not be increased whatever the size of the matrix, it will always behave as the BPSK mapping technique from the data rate point of view.

Let us have a look at the matrix (R), which is the 1D-IFFT for each column of the matrix (F_{opt}) before normalization. It always have element positive values between 0 and p related to the following examples:

$$Input\ Data\ D_{mn} = \begin{bmatrix} 0 & 0 & 0 \\ 0 & 0 & 0 \\ 0 & 0 & 0 \end{bmatrix} \Rightarrow R = \begin{bmatrix} 0 & 0 & 0 & 0 \\ 0 & 0 & 0 & 0 \\ 0 & 0 & 0 & 0 \end{bmatrix} \quad (72)$$

$$Input\ Data\ D_{mn} = \begin{bmatrix} 0 & 1 & 0 \\ 0 & 0 & 1 \\ 1 & 0 & 1 \end{bmatrix} \Rightarrow R = \begin{bmatrix} 1 & 1 & 1 & 1 \\ 1 & 2 & 1 & 3 \\ 2 & 1 & 2 & 0 \end{bmatrix} \quad (73)$$

$$Input\ Data\ D_{mn} = \begin{bmatrix} 1 & 1 & 1 \\ 1 & 1 & 1 \\ 1 & 1 & 1 \end{bmatrix} \Rightarrow R = \begin{bmatrix} 3 & 3 & 3 & 3 \\ 3 & 3 & 3 & 3 \\ 3 & 3 & 3 & 3 \end{bmatrix} \quad (74)$$

By normalization and converting into complex as mentioned above, all the sub-carriers will result in positive phase between $(0\ \&\ \pi/2)$ with positive real and imaginary values between

$$0 \rightarrow 1.7321 + 1.7321i \left(= \frac{3+3i}{\sqrt{3}} \right).$$

Having long data input with variety of bits that covers from [0 0 0 0 0 0 0 0 0] to [1 1 1 1 1 1 1 1 1], the signal constellation of the FRAT sub-carriers resulted from a prime numbers $(p=3,\ p=5\ \&\ p=7)$. It is worth mentioning that when using more matrices with different sizes, the cumulative number of constellation points show all the constellation resulted from each matrix size to produce the needed number of data sub-carriers, the constellation of the (N_d) sub-carriers includes the constellations in Fig. 10.

The differences in positions of constellation points related to the distance between the adjacent points of each matrix, which is $\left(d = 1/\sqrt{p} \right)$.

The signal constellation of the FRAT mapper is considered as rectangular mapping, which are compatible to M-Ary QAM rather than M-Ary PSK. Therefore, we will consider the comparison with M-QAM mapping techniques in the next part.

The spectral efficiency is $\eta = R_b / N_d f_{sc}$, where, the relationship between the input bits and the output symbols is as follows:

$$N_{Bits} = p^2, \qquad N_d = p(p+1)/2 \quad (75)$$

$$N_{Bits} = R_b \times T_t \Rightarrow R_b = \frac{p^2}{T_t} \quad (76)$$

$$\eta = \frac{R_b}{N_d f_{sc}} = \frac{p^2}{T_t} \frac{2}{p(p+1) f_{sc}} = \frac{2p^2}{p(p+1)} \frac{1}{T_t f_{sc}} \quad (77)$$

In the case of critical time-frequency density ($T_t f_{sc} = T_u f_{sc} = 1$), i.e., maximum spectral efficiency for the FRAT transform is given as follows:

$$\eta = 2\frac{p}{p+1} < 2 \quad (78)$$

From this equation, the spectral efficiency for all combinations that may be used in any system will not exceed 2, in the contrary of using the M-Ary mapping techniques that is increased as the level of mapping increased.
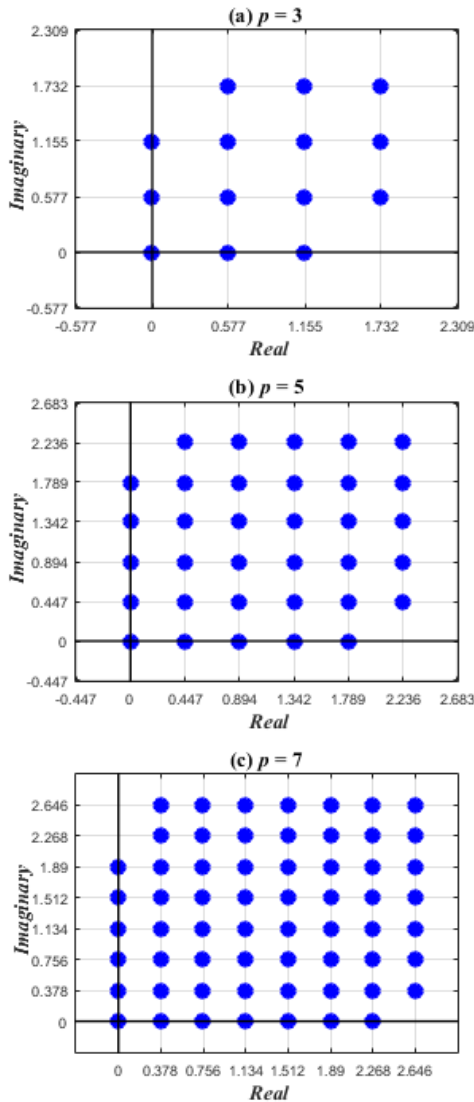

Fig. 10. FRAT Signal Constellation with Different Matrix Sizes

VI. CONCLUSIONS

In this paper detailed analysis of the equations used in RT and FRAT that explores the transformation and its inverse, which is appropriate to cope with images previously transformed with these approaches. The Fourier slice theorem is introduced showing the relationship between RT and the Fourier transform as well as the FRAT.

Extra analysis on FRAT is introduced showing how the optimal ordering is taken into consideration as well as generating the new normal vectors introduced by Do and Vetterli in [1]. This represents an introduction to construct complex data subcarriers from an input 2D matrix of binary numbers representing the input stream to an OFDM system.

The signal constellation of the output data subcarriers generated by FRAT is illustrated and the spectral efficiency using this constellation is introduced as an introduction to the second part of this research, which shows performance analysis of FRAT-based OFDM system.

REFERENCES

[1] M. N. Do and M. Vetterli, "The finite ridgelet transform for image representation," IEEE Transactions on Image Processing, vol. 12, no. 1, pp. 16-28, 2003.

[2] J. Radon, "On the determination of functions from their integral values along certain manifolds," IEEE Transactions on Medical Imaging, vol. 5, no. 4, pp. 170-176, 1986.

[3] H. H. Barrett, "Fundamentals of the Radon Transform," presented at the Mathematics and Computer Science in Medical Imaging, Berlin, Heidelberg, 1988.

[4] A. G. Ramm and A. I. Katsevich, The Radon Transform and Local Tomography, 1st ed ed. CRC Press. , 1996.

[5] S. Deans, The Radon Transform and Some of Its Applications. New Yourk: John Wiley and Sons Ltd 1983.

[6] H. H. Barrett, "III The Radon Transform and Its Applications," in Progress in Optics, vol. 21, E. Wolf, Ed.: Elsevier, 1984, pp. 217-286.

[7] G. Beylkin, "Discrete radon transform," IEEE Transactions on Acoustics, Speech, and Signal Processing, vol. 35, no. 2, pp. 162-172, 1987.

[8] Y. Gu and M. Sacchi, "Radon Transform Methods and Their Applications in Mapping Mantle Reflectivity Structure," Surveys in Geophysics, vol. 30, pp. 327-354, 10/01 2009.

[9] K. G. Samarah, S. Jones, and R. A. Abd-Alhameed, "Performance assessment of mobile OFDM-based systems: Variability within given wideband channel Categories," in Journal of Communications and Computer vol. 7, July 2014 ed, 2014, pp. 64 - 74.

[10] R. V. Nee and R. Prasad, OFDM for Wireless Multimedia communications. Boston; London: Artech House Publisher, 2000.

[11] R. Prasad, OFDM for Wireless Communications Systems. Artech House universal personal communications series 2004, p. 272.

[12] R. Lidl and H. Niederreiter, Introduction to Finite Fields and their Applications, 2 ed. Cambridge: Cambridge University Press, 1994.

[13] K. V. Hansen and P. A. Toft, "Fast curve estimation using preconditioned generalized Radon transform," IEEE Transactions on Image Processing, vol. 5, no. 12, pp. 1651-1661, 1996.

[14] G. Kertész, S. Szénási, and Z. Vámossy, "Application and properties of the radon transform for object image matching," in 2017 IEEE 15th International Symposium on Applied Machine Intelligence and Informatics (SAMI), 2017, pp. 000353-000358.

[15] H. TaiChiu, D. P. K. Lun, and S. Wan-Chi, "The discrete periodic Radon transform," IEEE Transactions on Signal Processing, vol. 44, no. 10, pp. 2651-2657, 1996.

[16] N. Ohyama, S. Ohki, S. Inoue, J. Tsujiuchi, and T. Honda, "Discrete Radon transform in a continuous space," Journal of the Optical Society of America A, vol. 4, no. 2, pp. 318-324, 1987/02/01 1987.

[17] B. Kelley and V. Madisetti, "The fast discrete Radon transform. I. Theory," IEEE transactions on image processing : a publication of the IEEE Signal Processing Society, vol. 2, pp. 382-400, 02/01 1993.

[18] I. Svalbe, "Image operations in discrete Radon space," pp. 21-22, 02/01 2002.

[19] M. R. Hejazi, G. Shevlyakov, and Y. Ho, "Modified Discrete Radon Transforms and Their Application to Rotation-Invariant Image Analysis," in 2006 IEEE Workshop on Multimedia Signal Processing, 2006, pp. 429-434.

[20] A. Kingston, "Orthogonal discrete Radon transform over pn×pn images," Signal Processing, vol. 86, no. 8, pp. 2040-2050, 2006/08/01/ 2006.

[21] D. F. Swinehart, "The Beer-Lambert Law," Journal of Chemical Education, vol. 39, no. 7, p. 333, 1962/07/01 1962.

[22] G. Beylkin, "Generalized Radon Transform and its Applications," 8227162 Ph.D., New York University, Ann Arbor, 1982.

[23] S. Helgason, The Radon Transform, 1 ed. (Progress in Mathematics). Springer, Boston, MA, 1999, pp. XIII, 193.

[24] J. S. Walker, Fast Fourier transforms, 2nd ed. (Studies in advanced mathematics). Boca Raton, Fla. ; London: CRC Press, 1996, pp. xv, 447.

[25] J. W. Cooley, Fast Fourier transform (FFT) (Encyclopedia of Computer Science). London: John Wiley and Sons Ltd., 1996, p. 4.

[26] R. N. Bracewell, The Fourier Transform And Its Applications. Tata Mcgraw-Hill Publishing Company Limited, 1987.

[27] R. N. Bracewell, "Numerical Transforms," Science, vol. 248, no. 4956, pp. 697-704, 1990/05/11 1990.

[28] R. Ng, "Fourier slice photography," ACM Trans. Graph., vol. 24, no. 3, pp. 735–744, 2005.

[29] S. Zhao and H. Halling, "A new Fourier method for fan beam reconstruction," in 1995 IEEE Nuclear Science Symposium and Medical Imaging Conference Record, 1995, vol. 2, pp. 1287-1291 vol.2.

[30] A. M. Grigoryan, "An algorithm of the two-dimensional Fourier transform," Radioelectronica Izvestiya VUZov SSSR, vol. 27, no. 10, pp. 52-57, 1984.

[31] G. Zeng, Y. Li, and A. Zamyatin, "Iterative total-variation reconstruction versus weighted filtered-backprojection reconstruction with edge-preserving filtering," Physics in medicine and biology, vol. 58, pp. 3413-3431, 04/26 2013.

[32] P. R. Edholm and G. T. Herman, "Linograms in image reconstruction from projections. 1. Back projecting using the Radon transform," in Proceedings of the Twenty-First Annual Hawaii International Conference on System Sciences, 1988. Vol.IV. Applications Track, 1988, vol. 4, pp. 48-50.

[33] M. L. Brady, "A Fast Discrete Approximation Algorithm for the Radon Transform," SIAM Journal on Computing, vol. 27, no. 1, pp. 107-119, 1998.

[34] D. Lun, T.-C. Hsung, and T. W. Shen, "Orthogonal discrete periodic Radon transform. Part I: Theory and realization," Signal Processing, vol. 83, pp. 941-955, 05/01 2003.

[35] D. P. K. Lun, T. C. Hsung, and T. W. Shen, "Orthogonal discrete periodic Radon transform: part II: applications," Signal Process., vol. 83, no. 5, pp. 957–971, 2003.

[36] E. D. Bolker, "The finite Radon transform," Contemp. Math, vol. 63, pp. 27-50, 1987.

[37] D. Persi and R. L. Graham, "The Radon transform on Z^k_2," Pacific Journal of Mathematics, vol. 118, no. 2, pp. 323-345, 1/1 1985.

[38] J. P. S. Kung, "Reconstructing finite radon transforms," Nuclear Physics B - Proceedings Supplements, vol. 5, no. 1, pp. 44-49, 1988/09/01/ 1988.

[39] F. Matus and J. Flusser, "Image representation via a finite Radon transform," IEEE Transactions on Pattern Analysis and Machine Intelligence, vol. 15, no. 10, pp. 996-1006, 1993.

[40] M. do and M. Vetterli, "Discrete Ridgelet Transforms for Image Representation," Audio-Visual Communications Laboratory (LCAV), 07/05 2010.

[41] A. Kingston and I. Svalbe, "Generalised finite radon transform for N×N images," Image and Vision Computing, vol. 25, no. 10, pp. 1620-1630, 2007/10/01/ 2007.

[42] M. N. Do and M. Vetterli, "Discrete ridgelet transforms for image representation," 2001.

[43] R. Lidl and H. Niederreiter, Introduction to finite fields and their applications. Cambridge University Press, 1986.

[44] M. N. Do and M. Vetterli, "Orthonormal finite ridgelet transform for image compression," in Proceedings 2000 International Conference on Image Processing (Cat. No.00CH37101), 2000, vol. 2, pp. 367-370 vol.2.

Khalid G. Samarah received the B.Sc. degree from Mutah University in Jordan in 1991, and the MSc and PhD from University of Bradford in UK in 2003 and 2007 respectively. From 17/02/2008, he worked as an Asociate Professor in Mutah University until now. Khalid occupied the position of head of the electrical engineering department in Mutah University, and chief of coordinators in the military wing of Mutah University. He is interesting in radio propagation, OFDM systems in cellular communications